

Microscopic origin of orbital magnetization in chiral superconductors

Jihang Zhu¹ and Chunli Huang²

¹*Department of Materials Science and Engineering, University of Washington, Seattle, Washington 98195, USA*

²*Department of Physics and Astronomy, University of Kentucky, Lexington, Kentucky 40506-0055, USA*

(Dated: January 21, 2026)

Chiral superconductivity is a time-reversal-symmetry-breaking superconducting phase that has attracted broad interest as a potential platform for topological quantum computation. A fundamental consequence of this symmetry breaking is orbital magnetization, yet a clear microscopic formulation of this quantity has remained elusive. This difficulty arises because Bogoliubov quasiparticles do not carry a definite electric charge, precluding a simple interpretation of orbital magnetization in terms of circulating quasiparticle currents. Moreover, superconductivity and ferromagnetism rarely coexist, and in the few materials where they do (e.g. uranium-based compounds), strong spin-orbit coupling obscures the orbital contribution to the magnetization. The recent report of chiral superconductivity in rhombohedral multilayer graphene, which has negligible spin-orbit coupling, therefore provides a unique opportunity to develop and test a microscopic theory of orbital magnetization in chiral superconductors. Here we develop such a theory, unifying the interband coherence effects underlying normal-state orbital magnetization with the intrinsic orbital moments of the Cooper-pair condensate, while fully respecting gauge invariance and conservation laws. Applying our theory to rhombohedral tetralayer graphene, we find that the onset of superconductivity can either enhance or suppress the normal-state orbital magnetization, depending sensitively on the bandstructure. We further identify a generalized clapping mode corresponding to coherent fluctuations between the two opposite chiral windings of the p -wave order parameter, $p \pm ip$, with a gap set by the sublattice winding form factor. This collective mode is unique to chiral superconductors and contributes to the orbital magnetization through its role in dressing the photon vertex. Experimental measurements of the orbital magnetization relative to the quarter-metal phase would provide a direct test of our theory.

INTRODUCTION

The Bardeen-Cooper-Schrieffer (BCS) theory [1], originally formulated for time-reversal-invariant superconductors, was soon generalized by Anderson and Morel [2] to higher-angular-momentum pairing states, including chiral phases that spontaneously break time-reversal symmetry. Despite decades of theoretical effort [3–11], however, formulating orbital magnetization in chiral superconductors at a microscopic level has proven conceptually challenging. One major reason is that much of the early theoretical understanding of orbital angular momentum in chiral superfluids, such as the $^3\text{He}-\text{A}$ phase, was developed in the context of translationally and Galilean-invariant systems. In such systems, spatial inhomogeneity arises only at sample boundaries where the order parameter necessarily vanishes, and boundary physics plays a subtle role in determining the orbital angular momentum and the associated edge currents [4, 6–8]. In crystalline superconductors, by contrast, Galilean invariance is explicitly broken by the periodic lattice potential, giving rise to an intrinsic bulk contribution to the orbital response. In particular, the velocity operator of crystalline material is not simply \mathbf{p}/m but consists of both the intraband Fermi velocity, $\nabla_{\mathbf{k}}\epsilon_F(\mathbf{k})/\hbar$, and the interband velocity matrix elements between Bloch states $\langle u_{c\mathbf{k}}|\mathbf{v}|u_{b\mathbf{k}}\rangle$. The interband matrix-elements are known to be essential in generating orbital magnetization even in normal (nonsuperconducting) crystals [12–17], making it natural, and necessary, to account for them in the superconducting phase.

This raises a fundamental question: how should we formulate orbital magnetization in a superconductor to consistently incorporate both the intrinsic orbital moment of Cooper pairs, which arises from pairing within a narrow energy window

around the Fermi surface, and the interband coherence induced by the periodic crystal potential, whose characteristic energy scales are typically much larger than the superconducting gap? Here we develop a microscopic theory that treats these two contributions on equal footing by moving beyond the traditional Fermi-surface-only description and systematically accounting for all virtual transitions between normal (Landau) quasiparticles and Bogoliubov quasiparticles, as shown in Fig. 1a. We then apply this framework to chiral superconductivity in rhombohedral tetralayer graphene, focusing on the quarter-metal phase [18], whose underlying bandstructure is relatively well understood. The quarter-metal phase is known to exhibit a strong anomalous Hall effect [19], and its orbital magnetization has been directly visualized using nano-SQUID measurements [20]. A central question, therefore, is how this orbital magnetization changes upon entering the superconducting state. We find that the effect of superconductivity on orbital magnetization depends sensitively on the normal-state bandstructure. Using a phenomenological attractive p -wave pairing model for rhombohedral tetralayer graphene, we show that when the quarter metal hosts three disjoint Fermi pockets, the onset of superconductivity enhances the orbital magnetization. By contrast, when the Fermi surface is simply connected, superconductivity suppresses the orbital magnetization. These contrasting behaviors lead to experimentally testable predictions that can be verified using combined nano-SQUID and quantum oscillation measurements.

In computing the dressed photon vertex, we identify a generalized clapping mode [21–30], corresponding to coherent fluctuations that reverse the superconducting chirality between the two discrete winding sectors. The mode has a finite gap set by the sublattice winding form factor, and its observation would

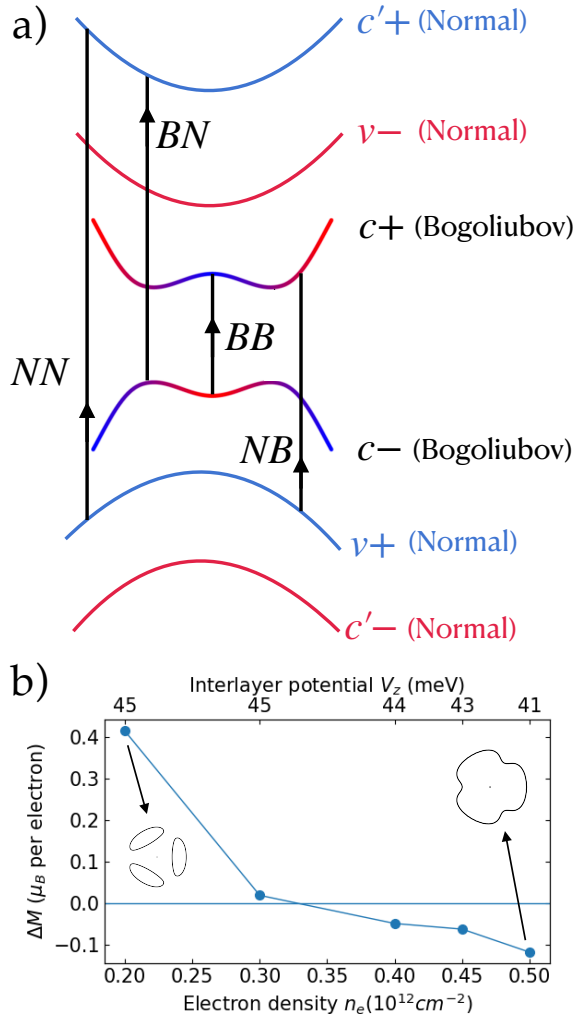


Figure 1. (a) Schematic illustration of the interband processes contributing to the orbital magnetization in a chiral superconductor, shown for a three-band model consisting of conduction bands c and c' , and a valence band v . Only the c band is superconducting, while the remaining bands remain in the normal state thus the transitions are classified according to whether the initial and final states are both normal-state quasiparticles (NN), both Bogoliubov quasiparticles (BB), or mixed normal–Bogoliubov states (NB and BN), see Sec. III for further discussion. (b) Orbital magnetization difference, ΔM , between the chiral p-wave superconducting and quarter-metal parent state as the carrier density and interlayer potential is tuned through a Lifshitz transition. The inset shows the Fermi-surface topology of the quarter-metal phase.

provide direct evidence for intrinsic chiral superconductivity in the quarter-metal phase.

MICROSCOPIC DERIVATION

We present a microscopic derivation of the orbital magnetization based on its thermodynamic definition and treats superconductivity within mean-field theory. A central result of our

approach is the identification of two distinct types of matrix elements: the photon vertex describing the electromagnetic coupling, and the quasiparticle velocity operator encoding the multiband structure of the Bogoliubov quasiparticles. The dressed photon vertex appears naturally in our microscopic theory and guarantees gauge invariance and current conservation. Our starting point is a generic microscopic $k \cdot p$ continuum Hamiltonian,

$$H = \sum_{\mathbf{k}\alpha\beta} \left[h_{\alpha\beta}(\mathbf{k}) \delta_{\mathbf{q},0} + \frac{e}{2} (\mathbf{v}_{\alpha\beta}(\mathbf{k}) + \mathbf{v}_{\alpha\beta}(\mathbf{k} + \mathbf{q})) \cdot \mathbf{A}_{\mathbf{q}} \right] c_{\mathbf{k}+\mathbf{q},\alpha}^\dagger c_{\mathbf{k}\beta} + \frac{1}{2} \sum_{\mathbf{k}\mathbf{k}'\mathbf{q}\alpha\beta} V_{\mathbf{k},\mathbf{k}'} c_{\mathbf{k}+\frac{\mathbf{q}}{2},\alpha}^\dagger c_{-\mathbf{k}+\frac{\mathbf{q}}{2},\beta}^\dagger c_{-\mathbf{k}'+\frac{\mathbf{q}}{2},\beta} c_{\mathbf{k}'+\frac{\mathbf{q}}{2},\alpha}. \quad (1)$$

Here $h_{\alpha\beta}(\mathbf{k})$ are matrix elements of a continuum $k \cdot p$ Hamiltonian and $\mathbf{v}(\mathbf{k}) = \nabla_{\mathbf{p}} h(\mathbf{p})|_{\mathbf{p}=\mathbf{k}}/\hbar$ represents the group-velocity operator of the Bloch waves. We apply minimal coupling to the Hamiltonian by introducing a vector potential $\mathbf{A}(\hat{\mathbf{r}}) = \mathbf{A}_{\mathbf{q}} e^{i\mathbf{q} \cdot \hat{\mathbf{r}}}$ that carries a single wavevector \mathbf{q} . Here $\hat{\mathbf{r}}$ is the position operator, α, β label orbital degrees of freedom of the electrons. For clarity, we consider spinless fermions and pairing at zero center-of-mass momentum. We then define the Nambu spinor

$$\Psi_{\mathbf{k}} = \begin{bmatrix} c_{\mathbf{k}\alpha_1} & \dots & c_{\mathbf{k}\alpha_N} & c_{-\mathbf{k}\alpha_1}^\dagger & \dots & c_{-\mathbf{k}\alpha_N}^\dagger \end{bmatrix}^T. \quad (2)$$

In this basis, the mean-field Hamiltonian can be written as

$$H = \frac{1}{2} \sum_{\mathbf{k},\mathbf{q}} \Psi_{\mathbf{k}+\mathbf{q}}^\dagger \left(H^{\text{BCS}}(\mathbf{k}) \delta_{\mathbf{q},0} + e \mathbf{A}_{\mathbf{q}} \cdot \Gamma_{\mathbf{k}}^0(\mathbf{q}) \right) \Psi_{\mathbf{k}}, \quad (3)$$

where the BCS mean-field Hamiltonian is

$$H^{\text{BCS}}(\mathbf{k}) = \begin{pmatrix} h(\mathbf{k}) & \Delta(\mathbf{k}) \\ \Delta^\dagger(\mathbf{k}) & -h^T(-\mathbf{k}) \end{pmatrix}, \quad (4)$$

and the pairing potential is $\Delta_{\alpha\beta}(\mathbf{k}) = \sum_{\mathbf{k}'} V_{\mathbf{k},\mathbf{k}'} \langle c_{-\mathbf{k}'\beta} c_{\mathbf{k}'\alpha} \rangle$. The photon-vertex is given by

$$\Gamma_{\mathbf{k}}^0(\mathbf{q}) = \begin{pmatrix} \frac{1}{2}(\mathbf{v}(\mathbf{k}) + \mathbf{v}(\mathbf{k} + \mathbf{q})) & 0 \\ 0 & -\frac{1}{2}(\mathbf{v}^T(-\mathbf{k}) + \mathbf{v}^T(-\mathbf{k} - \mathbf{q})) \end{pmatrix}. \quad (5)$$

Both the normal-state density matrix and the anomalous pairing amplitude can be described together using the quasiparticle density matrix $P = \sum_{\mathbf{k}} P(\mathbf{k})$, $P_{ij}(\mathbf{k}) = \langle \Psi_{\mathbf{k}j}^\dagger \Psi_{\mathbf{ki}} \rangle$ where i, j label components of the Nambu spinor. At self-consistency, the quasiparticle density matrix P satisfies the stationarity condition $[H^{\text{BCS}}(\mathbf{k}), P(\mathbf{k})] = 0, \forall \mathbf{k}$, and takes the form of a projector onto the occupied states,

$$P(\mathbf{k}) = \sum_i |U_{i\mathbf{k}}\rangle \langle U_{i\mathbf{k}}|, \quad H^{\text{BCS}}(\mathbf{k}) |U_{i\mathbf{k}}\rangle = E_{i\mathbf{k}} |U_{i\mathbf{k}}\rangle. \quad (6)$$

Throughout this work we use the notation

$$i, j : \text{occupied bands}, \quad m, n : \text{unoccupied bands}. \quad (7)$$

We caution the reader that the term “occupied state” in this context does not imply a fixed particle number, i.e. $\sum_{\mathbf{k}} \text{Tr}(P(\mathbf{k}))$

is not the total number of electrons because the BCS ground state is not a charge eigenstate. This language is used only to emphasize the analogy with the Hartree-Fock density matrix.

We now consider the perturbed ground state to linear order in the vector potential \mathbf{A}_q . The corresponding correction to the density matrix can be written as,

$$\delta P = \sum_{\mathbf{k}, m, i} X_{m\mathbf{k}+\mathbf{q}, i\mathbf{k}} |U_{m\mathbf{k}+\mathbf{q}}\rangle \langle U_{i\mathbf{k}}| + X_{i\mathbf{k}-\mathbf{q}, m\mathbf{k}} |U_{i\mathbf{k}-\mathbf{q}}\rangle \langle U_{m\mathbf{k}}|. \quad (8)$$

where $X \propto \mathbf{A}_q$ are linear-response coefficients. The resulting change in the grand potential is $\delta\Omega = \text{Tr}(\delta P \hat{\Omega})$,

$$\delta\Omega = \frac{1}{2} \sum_{\mathbf{k}mi} X_{m\mathbf{k}+\mathbf{q}, i\mathbf{k}} \langle U_{i\mathbf{k}} | \hat{\Omega} | U_{m\mathbf{k}+\mathbf{q}} \rangle + X_{i\mathbf{k}-\mathbf{q}, m\mathbf{k}} \langle U_{m\mathbf{k}} | \hat{\Omega} | U_{i\mathbf{k}-\mathbf{q}} \rangle. \quad (9)$$

Since the magnetic field is linear order in both \mathbf{A} and \mathbf{q} , we expand $\delta\Omega$ to first order in these quantities. Because the matrix elements $\langle U_{i\mathbf{k}} | \hat{\Omega} | U_{m\mathbf{k}+\mathbf{q}} \rangle$ vanish at $\mathbf{q} = 0$, the leading $O(Aq)$ contribution to $\delta\Omega$ must arise from the linear-in- q term of the expansion, $\langle U_{i\mathbf{k}} | \hat{\Omega} | U_{m\mathbf{k}+\mathbf{q}} \rangle = q_\mu \langle U_{i\mathbf{k}} | \partial_\mu U_{m\mathbf{k}} \rangle (E_{i\mathbf{k}} + E_{m\mathbf{k}})/2 + O(q^2)$. Retaining only this leading order, $\delta\Omega$ becomes

$$\delta\Omega = \frac{1}{2} \sum_{\mathbf{k}mi} (E_{m\mathbf{k}} + E_{i\mathbf{k}}) q_\mu \text{Re} [X_{m\mathbf{k}, i\mathbf{k}} \langle U_{i\mathbf{k}} | \partial_\mu U_{m\mathbf{k}} \rangle] + O(q^2) \quad (10)$$

and therefore only the coefficients X evaluated at $\mathbf{q} = 0$ are required. These coefficients are determined by the following linear equation from many-body perturbation theory [17, 31]:

$$(E_{m\mathbf{k}} - E_{i\mathbf{k}}) X_{m\mathbf{k}, i\mathbf{k}} - \delta\Sigma_{m\mathbf{k}, i\mathbf{k}} = -e \langle U_{m\mathbf{k}} | \Gamma_{\mathbf{k}}^0 | U_{i\mathbf{k}} \rangle \cdot \mathbf{A}, \quad (11)$$

where $\Gamma_{\mathbf{k}}^0$ is the bare photon vertex, obtained by setting $\mathbf{q} = 0$ in Eq. (5), and $\delta\Sigma$ is the induced self-energy. This equation represents a coupled linear system, since $\delta\Sigma$ generates transitions from other occupied states $|U_{j\mathbf{k}'}\rangle$ to unoccupied states $|U_{n\mathbf{k}'}\rangle$ with amplitudes $X_{n\mathbf{k}', j\mathbf{k}'}$. Solving this system amounts to resumming self-energy insertions into a renormalized photon vertex. The solution can be written in the following compact form,

$$X_{m\mathbf{k}, i\mathbf{k}} = \frac{-e \langle U_{m\mathbf{k}} | \Gamma_{\mathbf{k}} | U_{i\mathbf{k}} \rangle \cdot \mathbf{A}}{E_{m\mathbf{k}} - E_{i\mathbf{k}}}, \quad (12)$$

where $\Gamma_{\mathbf{k}}$ is the dressed photon vertex. Substituting this expression into Eq. (10), choosing a gauge with $A_\nu q_\mu = i\epsilon_{\nu\mu\lambda} B_\lambda/2$, and using the thermodynamic definition of the orbital magnetization $M_\lambda = -(\text{Area})^{-1} \partial\Omega/\partial B_\lambda$, we obtain

$$M_\lambda = \frac{e}{4} \int \frac{d^2\mathbf{k}}{4\pi^2} \sum_{mi} \frac{E_{m\mathbf{k}} + E_{i\mathbf{k}}}{E_{m\mathbf{k}} - E_{i\mathbf{k}}} \epsilon_{\lambda\mu\nu} \text{Im} [\langle U_{m\mathbf{k}} | \Gamma_{\mathbf{k}}^\nu | U_{i\mathbf{k}} \rangle \langle U_{i\mathbf{k}} | \partial_\mu U_{m\mathbf{k}} \rangle]. \quad (13)$$

Since $\langle U_{i\mathbf{k}} | H_{\mathbf{k}}^{\text{BCS}} | U_{m\mathbf{k}} \rangle = E_{m\mathbf{k}} \langle U_{i\mathbf{k}} | U_{m\mathbf{k}} \rangle = 0$, we can always

Operator	Normal State	Superconducting State
Bare velocity	$\mathbf{v}(\mathbf{k}) = \frac{1}{\hbar} \nabla_{\mathbf{k}} h(\mathbf{k})$	—
Quasiparticle velocity	$\frac{1}{\hbar} \nabla_{\mathbf{k}} H^{\text{HF}}(\mathbf{k})$	$\frac{1}{\hbar} \nabla_{\mathbf{k}} H^{\text{BCS}}(\mathbf{k})$
Bare photon vertex	$\mathbf{v}(\mathbf{k})$	$\Gamma_{\mathbf{k}}^0 = \begin{pmatrix} \mathbf{v}(\mathbf{k}) & 0 \\ 0 & -\mathbf{v}^T(-\mathbf{k}) \end{pmatrix}$
Dressed photon vertex	$\frac{1}{\hbar} \nabla_{\mathbf{k}} H^{\text{HF}}(\mathbf{k})$	$\Gamma_{\mathbf{k}} = (1 + \frac{C}{\Delta E})^{-1} \Gamma_{\mathbf{k}}^0$

Table I. Comparison of velocity and photon-vertex operators in the normal and superconducting states. In the normal state, the quasiparticle velocity and the dressed photon vertex coincide, reflecting charge conservation for Landau quasiparticles. In the superconducting state, these operators become distinct because Bogoliubov quasiparticles are not charge eigenstates. Here H^{HF} and H^{BCS} are the Hartree-Fock and BCS mean-field Hamiltonians.

relate the interband Berry connection to matrix elements of the mean-field quasiparticle velocity:

$$\langle U_{i\mathbf{k}} | \partial_\mu U_{m\mathbf{k}} \rangle = -\frac{\langle U_{i\mathbf{k}} | (\partial_\mu H^{\text{BCS}}(\mathbf{k})) | U_{m\mathbf{k}} \rangle}{E_{i\mathbf{k}} - E_{m\mathbf{k}}}. \quad (14)$$

This leads to our main result, which expresses M_λ in terms of the BCS quasiparticle energies and wave functions:

$$M_\lambda = \frac{e}{4} \int \frac{d^2\mathbf{k}}{(2\pi)^2} \sum_{mi} \frac{E_{m\mathbf{k}} + E_{i\mathbf{k}}}{(E_{m\mathbf{k}} - E_{i\mathbf{k}})^2} \epsilon_{\lambda\mu\nu} \times \text{Im} [\langle U_{m\mathbf{k}} | \Gamma_{\mathbf{k}}^\nu | U_{i\mathbf{k}} \rangle \langle U_{i\mathbf{k}} | (\partial_\mu H^{\text{BCS}}(\mathbf{k})) | U_{m\mathbf{k}} \rangle]. \quad (15)$$

This form of the orbital magnetization is very illuminating. The quantity M_λ depends on two types of transition matrix elements between occupied states i and unoccupied states m . The first is the dressed photon-vertex $\Gamma_{\mathbf{k}}^\nu$ which determines the electromagnetic response like the Meissner effect. The second is the Bogoliubov quasiparticle group-velocity operator $\partial_\mu H_{\mathbf{k}}^{\text{BCS}}$, which describes the propagation of quasiparticles in the superconducting state.

The important point is that, unlike in the normal state, Bogoliubov quasiparticles are not charge eigenstates. As a result, the group-velocity operator does not coincide with the photon vertex. By contrast, in the normal (non-superconducting) state, the solution of the linearized mean-field equation yields a photon vertex of the form $\Gamma_{\mathbf{k}}^\nu = \hbar^{-1} \partial_\nu H_{\mathbf{k}}^{\text{HF}}$ [17], which is identical to the quasiparticle group velocity. Substituting this relation and replacing H^{BCS} with H^{HF} , our expression reduces to the standard normal-state formula for orbital magnetization obtained from semiclassical theory. Physically, when Landau quasiparticles flow with a given velocity, they necessarily carry a corresponding charge current because they are charge eigenstates. This relationship is broken in the superconductor when Landau quasiparticles become Bogoliubov quasiparticles. A summary of these distinctions is in Table I.

For a superconductor with time-reversal symmetry, the quasiparticle energy $E_{n\mathbf{k}} = E_{-n\mathbf{k}}$, and both the photon vertex and the velocity operator are odd under time reversal. However, because time-reversal symmetry is antiunitary, it also

complex conjugates the matrix elements. Writing the quantity inside the imaginary part of Eq. (15), as $f(\mathbf{k})$, time reversal symmetry implies $\text{Im}(f(\mathbf{k})) = \text{Im}(f^*(-\mathbf{k}))$. Consequently, the integrand is an odd function of \mathbf{k} and vanishes upon integration over the whole Brillouin zone. Thus, the orbital magnetization vanishes in time-reversal symmetric superconducting state.

CHIRAL SUPERCONDUCTORS IN RHOMBOHEDRAL MULTILAYER GRAPHENE

Since the initial observation of superconductivity in rhombohedral trilayer graphene [32], many more superconducting phases has been identified in rhombohedral multilayer graphene [33–41]. Several of these phases are induced or enhanced by external magnetic fields [33, 37, 39–41], suggesting spin-polarized order-parameter, while others display unconventional directional responses [38]. Although the theoretical framework developed here applies broadly to these systems, we focus mainly here on the chiral superconductor whose parent state is an unambiguously symmetry-broken quarter metal with anomalous Hall effect. This is because this realizes a simple theoretical model of a single-component fermion, involving only a single valley, a single spin projection, and a single conduction band. A unique advantage of graphene-based superconductors compared to other candidate chiral superconductors is their relatively well understood electronic band structure, e.g. see Extended data Table 1 of Ref. [42]. For rhombohedral N -layer graphene, the low-energy electronic structure near a given valley is described by a $k \cdot p$ Hamiltonian with $2N$ bands,

$$h^{k \cdot p} = \sum_{n,\mathbf{k}} \xi_{n\mathbf{k}} |\phi_{n\mathbf{k}}\rangle \langle \phi_{n\mathbf{k}}|, \quad \xi_{n\mathbf{k}} = \epsilon_{n\mathbf{k}} - \mu. \quad (16)$$

We assume that superconductivity develops in the first conduction band label as c , and that the attractive interaction is much smaller than the spectral separation to other bands. Projecting onto this band yields the effective Hamiltonian

$$H_c = \sum_{\mathbf{k}} \xi_{c\mathbf{k}} a_{c\mathbf{k}}^\dagger a_{c\mathbf{k}} + \frac{1}{2} \sum_{\mathbf{k},\mathbf{k}'} \tilde{V}_{\mathbf{k},\mathbf{k}'} a_{c\mathbf{k}}^\dagger a_{c,-\mathbf{k}'}^\dagger a_{c,-\mathbf{k}'} a_{c\mathbf{k}'}, \quad (17)$$

$$\tilde{V}_{\mathbf{k},\mathbf{k}'} = V_{\mathbf{k},\mathbf{k}'} \langle \phi_{c,\mathbf{k}} | \phi_{c,\mathbf{k}'} \rangle \langle \phi_{c,-\mathbf{k}} | \phi_{c,-\mathbf{k}'} \rangle. \quad (18)$$

At present there is no consensus on the microscopic pairing mechanism in rhombohedral multilayer graphene [43–51], and identifying such a mechanism is not the goal of this work. Instead, our focus is to determine the orbital magnetization associated with a given superconducting state. We therefore introduce a phenomenological attractive interaction that favors p -wave pairing,

$$V_{\mathbf{k},\mathbf{k}'} = -\frac{g}{A} (e^{i\phi_{\mathbf{k}}} e^{-i\phi_{\mathbf{k}'}} + e^{-i\phi_{\mathbf{k}}} e^{i\phi_{\mathbf{k}'}}). \quad (19)$$

Here A denotes the system area, and we choose $g \sim 160 \text{ meV nm}^{-2}$, a value that yields a reasonable estimate of

the superconducting transition temperature and its density dependence [47]. In the case we study in the main text, the Fermi energy $\epsilon_F = 0.92 \text{ meV}$, $gn_e = 0.8 \text{ meV}$ and $gN_F = 0.5$ where N_F is the density-of-states at the Fermi level. We note when g is too small, superconductivity is no longer energetically favored and the system remains metallic despite the presence of an attractive interaction [47]. This is because pairing in a time-reversal symmetry-broken band does not give rise to the conventional BCS logarithmic divergence.

The mean-field approximation leads to the following BCS Hamiltonian for the conduction band,

$$H_c^{\text{BCS}}(\mathbf{k}) = \xi_{c,\mathbf{k}}^o - \mathbf{d}_{\mathbf{k}} \cdot \boldsymbol{\tau}, \quad (20)$$

$$\mathbf{d}_{\mathbf{k}} = -[\text{Re}(\Delta_{\mathbf{k}}), -\text{Im}(\Delta_{\mathbf{k}}), \xi_{c,\mathbf{k}}^e],$$

where $\boldsymbol{\tau}$ denotes Pauli matrices in Nambu space. $\xi_{c,\mathbf{k}}^o = (\xi_{c,\mathbf{k}} - \xi_{c,-\mathbf{k}})/2$ and $\xi_{c,\mathbf{k}}^e = (\xi_{c,\mathbf{k}} + \xi_{c,-\mathbf{k}})/2$ are the odd and even combination of band-dispersion. The superconducting gap $\Delta_{\mathbf{k}} = -\Delta_{-\mathbf{k}}$ is obtained self-consistently, as discussed in the Appendix, yielding the Bogoliubov quasiparticle energies $E_{\pm,c,\mathbf{k}}$ and eigenvectors $|U_{\pm,c,\mathbf{k}}\rangle$, where \pm label the electron-like and hole-like branches in the Nambu representation.

Fig 2a shows the Bogoliubov quasiparticle band dispersion for tetralayer graphene ($N = 4$) with the inset indicating the electron and hole Fermi surfaces. Fig 2b shows the phase winding of the $p - ip$ superconducting order parameter, which rotates by 2π upon traversing a closed loop counterclockwise in momentum space. Fig 2c plots the normalized Anderson pseudospin vector, $\hat{\mathbf{d}}_{\mathbf{k}} = \mathbf{d}_{\mathbf{k}}/|\mathbf{d}_{\mathbf{k}}|$, revealing a skyrmion-like texture. The associated Pontryagin index of the skyrmion ($C = -1$) is the topological invariant of the chiral superconductor. The out-of-plane pseudospin component $\hat{d}_{\mathbf{k}}^z$ encodes the joint occupation of states at \mathbf{k} and $-\mathbf{k}$: $\hat{d}_{\mathbf{k}}^z = 1$ indicates that both states are occupied, while $\hat{d}_{\mathbf{k}}^z = -1$ indicates that both are empty. In the normal state, $\hat{d}_{\mathbf{k}}^z$ exhibits a sharp domain wall at the Fermi surface, switching abruptly between ± 1 . In the superconducting state, pairing between \mathbf{k} and $-\mathbf{k}$ smooths this domain wall. Because the normal-state Fermi surface has only C_3 symmetry, $\epsilon_{\mathbf{k}} = \epsilon_{C_3\mathbf{k}}$, the resulting $\hat{d}_{\mathbf{k}}^z$ has a C_6 symmetry.

In rhombohedral multilayer graphene, however, $\hat{d}_{\mathbf{k}}^z$ still varies sharply in momentum space near the overlap of the electron and hole Fermi surfaces. This behavior originates from the unusual normal-state dispersion, which is exceptionally flat near the K point but rises rapidly at larger $|\mathbf{k}|$, producing the so-called “Berry-trashcan” profile [44]. As we show below, this distinctive pseudospin structure plays a central role in determining the orbital magnetization of the superconducting state in rhombohedral multilayer graphene.

Although our phenomenological interaction V [Eq. (19)] does not energetically distinguish between $p + ip$ over $p - ip$ pairing, the sublattice winding encoded in the form factors in \tilde{V} selects a definite chirality [52]. The resulting energy splitting between the two chiral states, however, remains small; for the case shown in Fig. 2, it is approximately $44 \mu\text{eV}$ per electron. For valley K , where the intralayer hopping between sublattices

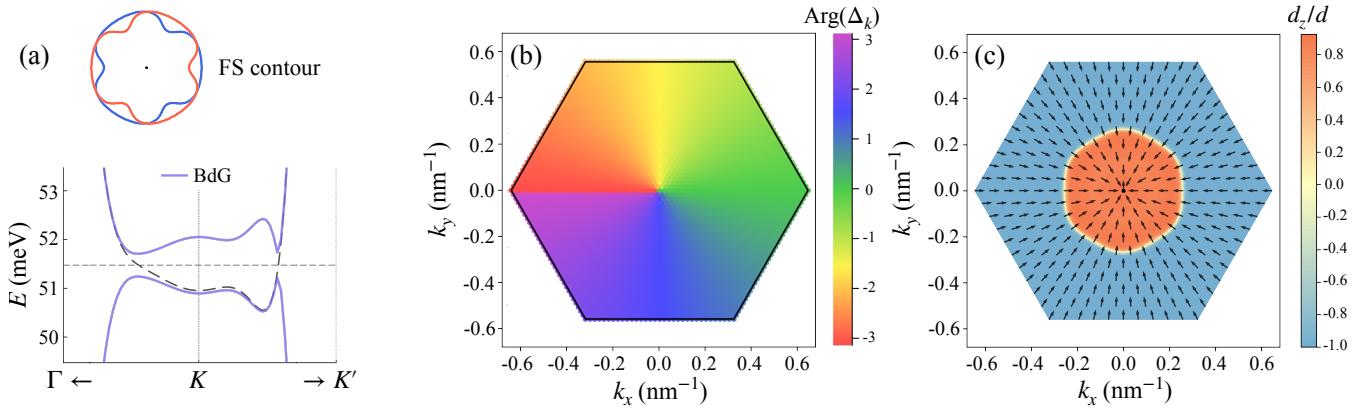


Figure 2. Superconducting ground state of rhombohedral tetralayer graphene in valley K at $V_z = 41$ meV and carrier density $n_e = 0.5 \times 10^{12} \text{ cm}^{-2}$, corresponding to the highest-density point shown in Fig. 1b). (a) Fermi-surface contours of $\xi_{c,\mathbf{k}}$ (blue) and $\xi_{c,-\mathbf{k}}$ (orange), together with the self-consistent Bogoliubov–de Gennes spectrum. The black dashed curve shows the normal-state conduction-band dispersion, and the gray dashed horizontal line indicates the Fermi level. (b) Phase of the superconducting order parameter $\Delta_{\mathbf{k}}$. (c) Skyrmiон-like texture of the pseudospin field $\mathbf{d}_{\mathbf{k}}$, with the in-plane components (d_x, d_y) shown as arrows and the out-of-plane component d_z encoded in the color scale. The in-plane components are normalized by $(d_x^2 + d_y^2)^{1/2}$, and d_z is normalized by the total magnitude $d = (d_x^2 + d_y^2 + d_z^2)^{1/2}$. All calculations are performed using an interaction strength $g = 160 \text{ meV}\cdot\text{nm}^2$, chosen to reproduce the experimentally observed critical temperature.

is $\langle A_1 | T | B_1 \rangle = \hbar v_F (\tau k_x + i k_y)$ with $\tau = +1$, the energetically favored state has $p - ip$ chirality.

This mean-field solution provides the basis for analyzing the orbital magnetization M_z . In the superconducting state, M_z receives contributions from interband virtual transitions involving either normal-state quasiparticles or Bogoliubov quasiparticles. Accordingly, these processes fall into three classes: normal–normal (NN), normal–Bogoliubov (NB and BN), and Bogoliubov–Bogoliubov (BB), as indicated by the arrows in Fig. 1a.

$$M_z = \int \frac{d^2\mathbf{k}}{4\pi^2} \left[M_z^{NN}(\mathbf{k}) + M_z^{NB}(\mathbf{k}) + M_z^{BN}(\mathbf{k}) + M_z^{BB}(\mathbf{k}) \right]. \quad (21)$$

Figure 1a schematically illustrates these contributions. The outer bands, labeled $c'+$ and $v+$, represent normal-state electron bands together with their corresponding Nambu hole partners $c'-$ and $v-$. The two central bands, denoted $c\pm$, are Bogoliubov quasiparticle bands generated by superconducting pairing.

In the following, we focus on the highest-density point shown in Fig. 1, whose superconducting solution is analyzed in detail in Fig. 2; results for the remaining density points are presented in Appendix.

Normal-normal (NN) transitions

The normal-normal contribution is the simplest: it consists of transitions from all valence bands of $h^{K,p}$ to all non-superconducting conduction bands $c' \neq c$. In the general expression Eq. (15), this corresponds to choosing initial state $i = (v, +)$ and final state $m = (c', +)$, with v running over all valence bands and $c' \neq c$ running over all conduction bands

except the one participating in superconductivity. An equivalent set of contributions arises from choosing $i = (c', -)$ and $m = (v, -)$, which describe the same virtual processes in the hole sector of the Nambu representation. Because these two descriptions are related by particle–hole conjugation, they yield identical contributions. Adding both, we obtain

$$M_z^{NN}(\mathbf{k}) = \frac{e}{2\hbar} \sum_{c' \neq c} \sum_v \frac{\xi_{c'\mathbf{k}} + \xi_{v\mathbf{k}}}{(\xi_{c'\mathbf{k}} - \xi_{v\mathbf{k}})^2} \epsilon_{\mu\nu} \times \text{Im} \left(\langle \phi_{c'\mathbf{k}} | (\partial_\nu h(\mathbf{k})) | \phi_{v\mathbf{k}} \rangle \langle \phi_{v\mathbf{k}} | (\partial_\mu h(\mathbf{k})) | \phi_{c'\mathbf{k}} \rangle \right). \quad (22)$$

This contribution is entirely determined by the normal-state band structure and is unaffected by superconductivity. It therefore represents a background orbital magnetization inherited from the normal parent state. The \mathbf{k} -space distribution is shown in Fig. 3a, the large contribution comes from the zone corner ($k_x = k_y = 0$) because the Berry curvature is strongest over there.

Mixed Normal–Bogoliubov Transitions (NB and BN)

The next class consists of transitions between a normal Landau quasiparticle and a Bogoliubov quasiparticle. These processes are the primary mechanism by which superconductivity modifies the orbital magnetization inherited from the normal state. We first consider processes in which the initial states are normal Landau quasiparticles $i = (v, +)$ and the final state is fixed to be an unoccupied Bogoliubov quasiparticle band $m = (c, +)$. Here v runs over all valence bands, while c denotes the conduction band that participates in superconductivity. We denote this contribution by M_z^{NB} . There is no vertex correction in this channel, since the pairing self-energy has

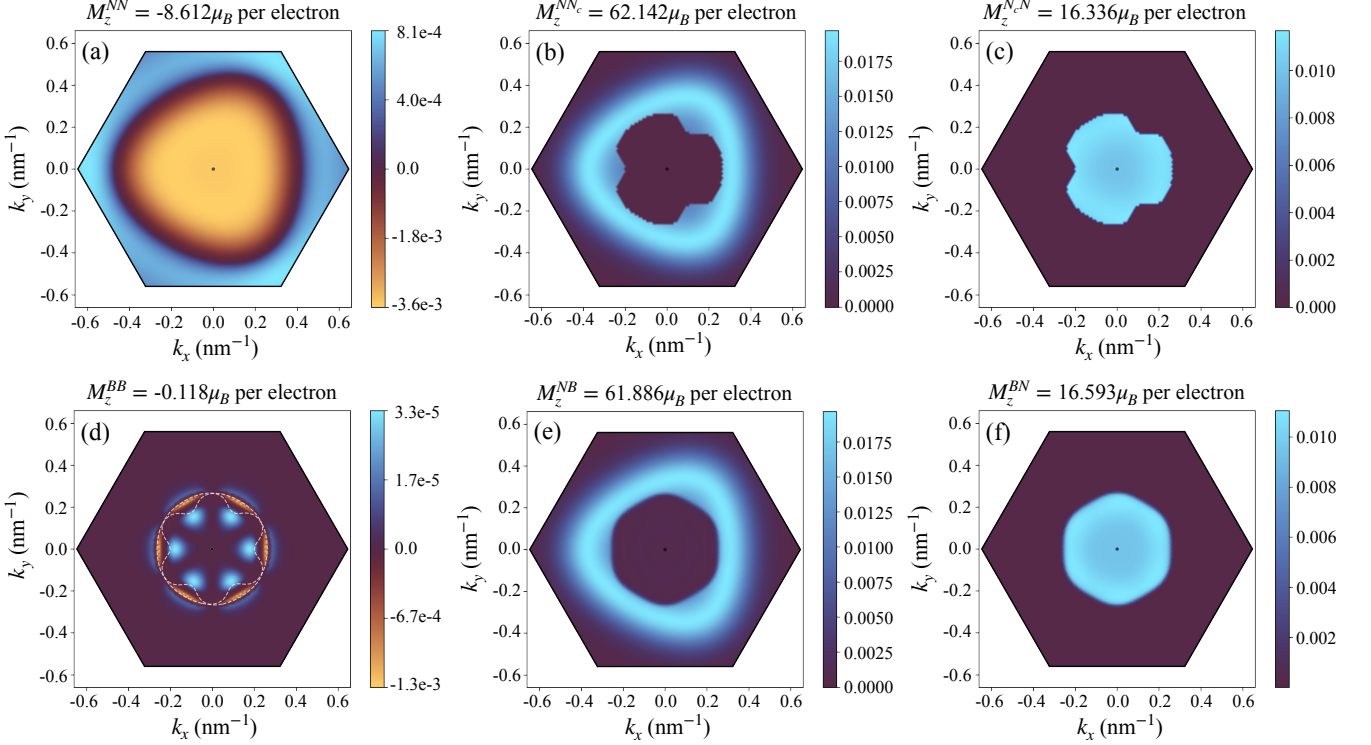


Figure 3. Momentum-space distributions of the orbital magnetization contributions from the normal–normal, mixed (NB and BN), and Bogoliubov–Bogoliubov channels: (a) $M_z^{NN}(\mathbf{k})$, (b) $M_z^{NNc}(\mathbf{k})$, (c) $M_z^{NcN}(\mathbf{k})$, (d) $M_z^{BB}(\mathbf{k})$, (e) $M_z^{NB}(\mathbf{k})$, and (f) $M_z^{BN}(\mathbf{k})$, shown in units of μ_B per electron for rhombohedral tetralayer graphene in valley K at $V_z = 41$ meV and carrier density $n_e = 0.5 \times 10^{12} \text{ cm}^{-2}$. The total orbital magnetization obtained by summing over \mathbf{k} is indicated in the title of each panel. In panel (d), the color scale spans the minimum and maximum values of $M_z^{BB}(\mathbf{k})$; note that the peak magnitude is nearly two orders of magnitude larger than the background, so the dominant contribution originates from the region where the electron and hole Fermi surfaces overlap, shown as the dashed white contours. By contrast, the mixed NB and BN contributions arise from the entire Fermi sea rather than being confined to the Fermi-surface region.

no matrix elements connecting these sets of bands. By particle–hole symmetry, there is an identical contribution from the hole sector obtained by taking $i = (c, -)$ and $m = (v, -)$. Summing both contributions yields

$$M_z^{NB}(\mathbf{k}) = \frac{e}{2\hbar} \sum_v \left[\frac{E_{c,+,\mathbf{k}} + \xi_{v\mathbf{k}}}{(E_{c,+,\mathbf{k}} - \xi_{v\mathbf{k}})^2} \sin^2\left(\frac{\theta_{\mathbf{k}}}{2}\right) \epsilon_{\mu\nu} \right. \\ \left. \text{Im} \left(\langle \phi_{c\mathbf{k}} | (\partial_\nu h(\mathbf{k})) | \phi_{v\mathbf{k}} \rangle \langle \phi_{v\mathbf{k}} | (\partial_\mu h(\mathbf{k})) | \phi_{c\mathbf{k}} \rangle \right) \right]. \quad (23)$$

It is instructive to examine how this expression reduces to the normal-state result in the limit of vanishing superconductivity. In this limit, the Anderson pseudospin [53] becomes a sharp domain wall at the Fermi surface, with $\theta_{\mathbf{k}} = \pi$ for unoccupied states and $\theta_{\mathbf{k}} = 0$ for occupied states. Consequently, the BCS probability factor for the Bogoliubov final state to be empty reduces to $\sin^2(\theta_{\mathbf{k}}/2) \rightarrow \Theta(\xi_{c\mathbf{k}})$, where $\Theta(x)$ is the Heaviside step function, while the Bogoliubov quasiparticle energy approaches the normal-state band energy, $E_{c,+,\mathbf{k}} \rightarrow \xi_{c\mathbf{k}}$. Implementing these substitutions, $M_z^{NB}(\mathbf{k})$ reduces identically to

the normal-state contribution, which we denote by $M_z^{NNc}(\mathbf{k})$:

$$M_z^{NNc}(\mathbf{k}) = \frac{e}{2\hbar} \sum_v \left[\frac{\xi_{c\mathbf{k}} + \xi_{v\mathbf{k}}}{(\xi_{c,\mathbf{k}} - \xi_{v\mathbf{k}})^2} \Theta(\xi_{c\mathbf{k}}) \epsilon_{\mu\nu} \right. \\ \left. \text{Im} \left(\langle \phi_{c\mathbf{k}} | (\partial_\nu h(\mathbf{k})) | \phi_{v\mathbf{k}} \rangle \langle \phi_{v\mathbf{k}} | (\partial_\mu h(\mathbf{k})) | \phi_{c\mathbf{k}} \rangle \right) \right]. \quad (24)$$

This term corresponds to interband transitions from all filled valence bands into the conduction band c that hosts a Fermi surface. These contributions are shown in Fig. 3b and e for comparison. In the normal state, $M_z^{NNc}(\mathbf{k})$ vanishes for momenta inside the trigonally warped Fermi surface because of the strict Pauli blocking of interband processes into already occupied final states. In the superconducting phase, the BCS occupation factor $\sin^2(\theta_{\mathbf{k}}/2) = (1 - d_{\mathbf{k}}^2/d_{\mathbf{k}})/2$, softens this Pauli constraint and has a C_6 symmetry. For the value of g chosen to reproduce the experimental T_c , $\sin^2(\theta_{\mathbf{k}}/2)$ varies rapidly from 0 to 1 in the momentum region where the electron and hole Fermi surfaces overlap. As a result, the available phase space for interband transitions is overall reduced, leading to a suppression of the orbital magnetization in this channel. Quantitatively, we find $M_z^{NB} - M_z^{NNc} = -0.256 \mu_B$ per electron.

We next consider the complementary BN processes, in which the initial state is the empty (lower) Bogoliubov quasiparticle band $i = (c, -)$ and the final states are normal conduction bands $m = (c', +)$ with $c' \neq c$. We denote this contribution by M_z^{BN} . Proceeding analogously, we obtain

$$M_z^{BN}(\mathbf{k}) = \frac{e}{2\hbar} \sum_{c' \neq c} \left[\frac{E_{c,-,\mathbf{k}} + \xi_{c'\mathbf{k}}}{(E_{c,-,\mathbf{k}} - \xi_{c'\mathbf{k}})^2} \cos^2\left(\frac{\theta_{\mathbf{k}}}{2}\right) \epsilon_{\mu\nu} \right. \\ \left. \text{Im}(\langle \phi_{c'\mathbf{k}} | (\partial_{\nu} h(\mathbf{k})) | \phi_{c\mathbf{k}} \rangle \langle \phi_{c\mathbf{k}} | (\partial_{\mu} h(\mathbf{k})) | \phi_{c'\mathbf{k}} \rangle) \right]. \quad (25)$$

In the limit of vanishing superconductivity, the BCS probability for the initial state to be occupied reduces to $\cos^2(\theta_{\mathbf{k}}/2) \rightarrow 1 - \Theta(\xi_{c,\mathbf{k}})$ and the Bogoliubov quasiparticle energy becomes the normal state energy $E_{c,-,\mathbf{k}} \rightarrow \xi_{c\mathbf{k}}$. With these substitutions, $M_z^{BN}(\mathbf{k})$ reduces to a normal-state contribution, which we denote by $M_z^{N_c N}(\mathbf{k})$,

$$M_z^{N_c N}(\mathbf{k}) = \frac{e}{2\hbar} \sum_{c' \neq c} \left[\frac{\xi_{c\mathbf{k}} + \xi_{c'\mathbf{k}}}{(\xi_{c\mathbf{k}} - \xi_{c'\mathbf{k}})^2} [1 - \Theta(\epsilon_{c,\mathbf{k}} - \epsilon_F)] \epsilon_{\mu\nu} \right. \\ \left. \text{Im}(\langle \phi_{c'\mathbf{k}} | (\partial_{\nu} h(\mathbf{k})) | \phi_{c\mathbf{k}} \rangle \langle \phi_{c\mathbf{k}} | (\partial_{\mu} h(\mathbf{k})) | \phi_{c'\mathbf{k}} \rangle) \right]. \quad (26)$$

These contributions are shown in Fig. 3c and f. Note that $M_z^{N_c N}(\mathbf{k})$ is finite only for momenta that are occupied in the first conduction band. In the superconducting phase, this strict Pauli constraint is relaxed by the BCS probability factor, allowing contributions from a broader range of momenta. As a result, the available phase space for interband transitions is overall increased, leading to a increased of the orbital magnetization in this channel, yielding $M_z^{BN} - M_z^{N_c N} = +0.256 \mu_B$ per electron.

Remarkably, this enhancement nearly compensates the suppression found in the NB process, such that the total mixed contribution remains roughly unchanged $M_z^{BN} + M_z^{NB} \sim M_z^{N_c N} + M_z^{NN_c}$. In summary, for the single-Fermi-surface case considered here, the mixed normal-Bogoliubov contributions have negligible net effect on the orbital magnetization. The dominant modification arises from the intrinsic contribution of Cooper pairs, which we discuss next.

Bogoliubov-Bogoliubov (BB) transitions

The Bogoliubov-Bogoliubov (BB) transitions describe the interband processes that occur entirely within the superconducting quasiparticle sector. These processes reflect the contribution to the orbital magnetization that arises from the Cooper pairs themselves. This contribution is obtained by setting $m = (c, +)$ and $i = (c, -)$ in Eq. (15), which yields

$$M_z^{BB}(\mathbf{k}) = \frac{e}{4} \frac{E_{c,+\mathbf{k}} + E_{c,-\mathbf{k}}}{(E_{c,+\mathbf{k}} - E_{c,-\mathbf{k}})^2} \epsilon_{\mu\nu} \\ \text{Im} \left(\langle U_{c,+\mathbf{k}} | \Gamma_{\mathbf{k}}^{\nu} | U_{c,-\mathbf{k}} \rangle \langle U_{c,-\mathbf{k}} | (\partial_{\mu} H_c^{\text{BCS}}(\mathbf{k})) | U_{c,+\mathbf{k}} \rangle \right). \quad (27)$$

Here $H_c^{\text{BCS}}(\mathbf{k})$ is the conduction-band BCS Hamiltonian introduced in Eq. (20), and $|U_{c,\pm,\mathbf{k}}\rangle$ and $E_{c,\pm,\mathbf{k}}$ are its eigenstates and eigenvalues. The only undetermined quantity in Eq. (27) is the dressed photon vertex $\Gamma_{\mathbf{k}}$. A correct description of the orbital magnetization carried by Cooper pairs requires the inclusion of this dressed photon vertex in order to preserve gauge invariance and ensure charge conservation. Determining $\Gamma_{\mathbf{k}}$ is equivalent to solving the linearized time-dependent Bogoliubov-de Gennes equations, or, equivalently, diagonalizing the associated stability matrix. We describe the calculation of $\Gamma_{\mathbf{k}}$ in the next section, and present the resulting M_z^{BB} in Fig. 3(d). Unlike the mixed NB and BN contributions, where superconductivity enters only through quasiparticle energies and occupation factors, the BB contribution depends explicitly on the chirality of the superconducting order parameter. For the single Fermi-surface considered here, this contribution leads to an overall suppression of the orbital magnetization by approximately $0.118 \mu_B$ per electron. Because the mixed contributions approximately cancel, $M_z^{BN} + M_z^{NB} \approx M_z^{N_c N} + M_z^{NN_c}$, the net change in orbital magnetization caused by superconductivity is dominated by the contribution from the Cooper pairs themselves, M_z^{BB} . However, this behavior is not generic. At lower carrier densities, where the single Fermi surface undergoes a Lifshitz transition and splits into three pockets, M_z^{BB} becomes negligible. In this regime, the net enhancement of the orbital magnetization arises primarily from the mixed contributions, $M_z^{BN} + M_z^{NB} - (M_z^{N_c N} + M_z^{NN_c}) \approx 0.4 \mu_B$, see Appendix. This leads to the result shown in Fig. 1b.

An important message of Fig. 1 is that the momentum-space structure reveals a clear separation between Fermi-sea and Fermi-surface contributions: the mixed terms M_z^{NB} and M_z^{BN} are sensitive to the entire Fermi sea, whereas M_z^{BB} is strongly peaked around the overlap region of the electron and hole Fermi surfaces. The latter is consistent with the physical intuition that the intrinsic orbital magnetization of Cooper pairs is dominated by states near the Fermi surface.

GENERALIZED CLAPPING MODE

To determine the contribution of Cooper pairs to the orbital magnetization, we must compute the dressed photon vertex $\Gamma_{\mathbf{k}}$. This renormalization originates from collective excitations of the superconducting order parameter, which can be viewed as fluctuations of the Anderson pseudospin texture $\mathbf{d}_{\mathbf{k}}$. As we show below, the relevant collective modes correspond to chirality-flipping distortions of this texture, and is termed generalized clapping mode. We begin by simplifying Eq. (11), which can be recast in the compact matrix form

$$\sum_{\mathbf{k}'} \mathcal{S}_{\mathbf{k},\mathbf{k}'} \begin{pmatrix} X_{\mathbf{k}'}^R \\ X_{\mathbf{k}'}^I \end{pmatrix} = \begin{pmatrix} -e \gamma_{\mathbf{k}}^0 \cdot \mathbf{A} \\ 0 \end{pmatrix}, \\ \mathcal{S}_{\mathbf{k},\mathbf{k}'} = \Delta E_{\mathbf{k}} \delta_{\mathbf{k}\mathbf{k}'} \mathcal{I}_2 + C_{\mathbf{k},\mathbf{k}'}, \quad (28)$$

$$\gamma_{\mathbf{k}}^0 \equiv \frac{\mathbf{v}_{cc}(\mathbf{k}) + \mathbf{v}_{cc}(-\mathbf{k})}{2} \sin \theta_{\mathbf{k}}.$$

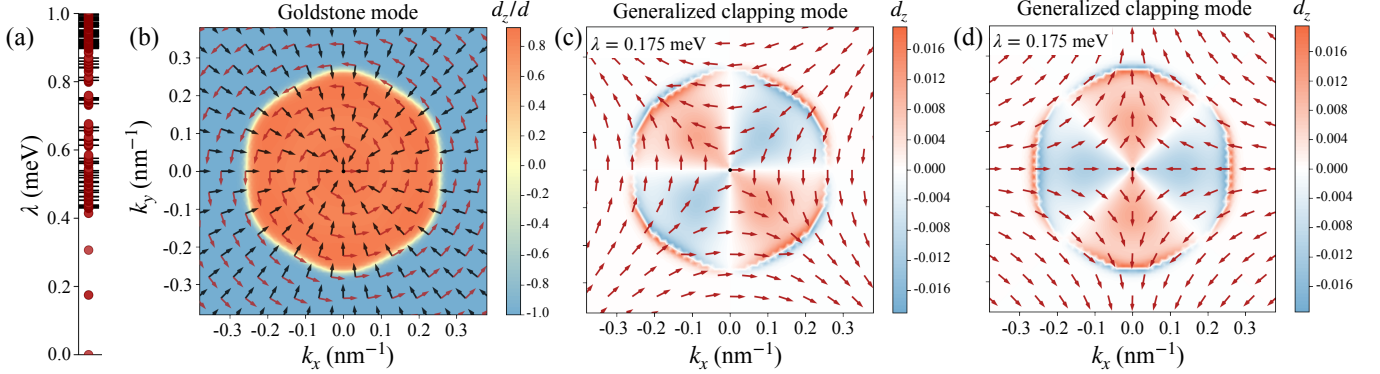


Figure 4. (a) Eigenvalues λ of the stability matrix \mathcal{S} (red dots) and $\Delta E_{\mathbf{k}}$ (black dash) in Eq. (28). (b) The Goldstone mode (red arrows) superimposed on top of the groundstate pseudospin distribution (black arrows) (c-d) The pseudospin distribution of the two degenerate generalized clapping modes, which have chirality opposite ($p + ip$) to that of the groundstate ($p - ip$).

Here I_2 is the 2×2 identity matrix and $X_{c,+,\mathbf{k};c-,\mathbf{k}} \equiv X_{\mathbf{k}}^R + i X_{\mathbf{k}}^I$ parameterizes interband response between the two Bogoliubov bands. The matrix \mathcal{S} plays the role of a stability matrix: its eigenvalues determine the spectrum of collective excitations of the superconducting state. The first term in \mathcal{S} is the \mathbf{k} -local Bogoliubov quasiparticle gap $\Delta E_{\mathbf{k}} = E_{c,+,\mathbf{k}} - E_{c,-,\mathbf{k}}$, while the second term

$$C_{\mathbf{k},\mathbf{k}'} = \tilde{V}_{\mathbf{k}\mathbf{k}'}^R \begin{pmatrix} \mathbf{a}_{\mathbf{k}} \cdot \mathbf{a}_{\mathbf{k}'} & \mathbf{a}_{\mathbf{k}} \cdot \mathbf{b}_{\mathbf{k}'} \\ \mathbf{b}_{\mathbf{k}} \cdot \mathbf{a}_{\mathbf{k}'} & \mathbf{b}_{\mathbf{k}} \cdot \mathbf{b}_{\mathbf{k}'} \end{pmatrix} + \tilde{V}_{\mathbf{k}\mathbf{k}'}^I \begin{pmatrix} \mathbf{a}_{\mathbf{k}} \times \mathbf{a}_{\mathbf{k}'} & \mathbf{a}_{\mathbf{k}} \times \mathbf{b}_{\mathbf{k}'} \\ \mathbf{b}_{\mathbf{k}} \times \mathbf{a}_{\mathbf{k}'} & \mathbf{b}_{\mathbf{k}} \times \mathbf{b}_{\mathbf{k}'} \end{pmatrix}. \quad (29)$$

encodes self-energy-induced vertex corrections. The vectors $\mathbf{a}_{\mathbf{k}}$ and $\mathbf{b}_{\mathbf{k}}$ originate from interband Pauli-matrix elements between the two Bogoliubov bands,

$$\tau_{+-}^{\alpha}(\mathbf{k}) \equiv \langle U_{c,+,\mathbf{k}} | \tau^{\alpha} | U_{c,-,\mathbf{k}} \rangle = a_{\mathbf{k}}^{\alpha} + i b_{\mathbf{k}}^{\alpha}, \quad (30)$$

where $\alpha = (x, y)$, and $a_{\mathbf{k}}^{x,y}$ and $b_{\mathbf{k}}^{x,y}$ are real. For a given pseudospin direction $\hat{d}_{\mathbf{k}}$, the unit vectors $\mathbf{e}_1(\mathbf{k})$ and $\mathbf{e}_2(\mathbf{k})$ span the tangent plane of the Bloch sphere. The vectors $\mathbf{a}_{\mathbf{k}} = P_{xy}\mathbf{e}_1(\mathbf{k})$ and $\mathbf{b}_{\mathbf{k}} = P_{xy}\mathbf{e}_2(\mathbf{k})$ are simply the projections of these tangent vectors onto the (particle-hole mixing) xy plane since the pairing self-energy lies entirely within this plane (see Appendix for details). In the language of time-dependent mean-field, the C matrix element encodes the effective interaction between two Bogoliubov quasiparticles with zero center-of-mass momentum, $\gamma_{\mathbf{k}}^{\dagger}\gamma_{-\mathbf{k}}^{\dagger}$ created out of the BCS vacuum. When $\mathbf{a}_{\mathbf{k}}$ and $\mathbf{b}_{\mathbf{k}}$ are parallel, the two Bogoliubov quasiparticles experience attractive matrix elements from the real part \tilde{V}^R . When they are orthogonal, they scatter with the imaginary part of the matrix elements. We note that $\tilde{V}^I = 0$ only for time-reversal-symmetric pairing.

The eigenvalue spectrum of \mathcal{S} is shown in Fig. 4a. The black dashed line corresponds to the energy of two uncoupled Bogoliubov quasiparticles propagating independently, obtained by setting $C = 0$. In this limit no collective modes are present and the spectrum consists of a continuum starting at 2Δ . The red points show the spectrum for $C \neq 0$, where the most prominent feature is the emergence of discrete collective modes below the continuum. We can visualize the wavefunction of the

collective mode through the associated pseudospin distribution,

$$\delta \mathbf{d}_{\mathbf{k}} = 2[\delta F_{\mathbf{k}}^R, -\delta F_{\mathbf{k}}^I, X_{\mathbf{k}}^R \sin \theta_{\mathbf{k}}], \quad (31)$$

where the real and imaginary components of the pairing-amplitude fluctuation are given by $\delta F_{\mathbf{k}}^R = X_{\mathbf{k}}^R a_{\mathbf{k}}^x + X_{\mathbf{k}}^I b_{\mathbf{k}}^x$ and $\delta F_{\mathbf{k}}^I = -X_{\mathbf{k}}^R a_{\mathbf{k}}^y - X_{\mathbf{k}}^I b_{\mathbf{k}}^y$.

The zero-energy mode corresponds to the Anderson-Bogoliubov-Goldstone (ABG) mode. In Fig. 4b, we plot the corresponding pseudospin texture $\delta \mathbf{d}_{\mathbf{k}}^{\text{ABG}}$ (red arrows) superimposed on the ground-state texture $\mathbf{d}_{\mathbf{k}}$ (black arrows). The ABG mode represents a global rotation of $\mathbf{d}_{\mathbf{k}}$, such that $\delta \mathbf{d}_{\mathbf{k}}^{\text{ABG}}$ is locally orthogonal to the ground-state pseudospin configuration. Fig. 4c and d show a pair of degenerate collective modes at energy $\lambda = 0.175$ meV, which are generalized clapping mode. The associated pseudospin texture, $\delta \mathbf{d}_{\mathbf{k}}^{\text{GCM}}$, corresponds to a p -wave order parameter with winding opposite to that of the ground state $\mathbf{d}_{\mathbf{k}}$. This is consistent with our mean-field analysis, which finds that the opposite-chirality configuration constitutes a locally stable solution, but with slightly higher energy due to the sublattice winding encoded in the form factors. The generalized clapping mode therefore describes collective fluctuations from the energetically preferred chirality, $p - ip$ to the unfavored higher-energy chirality in valley K ; in the opposite valley, the preferred chirality is reversed. The preferred chirality changes. In our pairing model, the excitation gap of this mode is set by the sublattice winding form factors and consequently exhibits layer dependence. This behavior is generic to interaction models that do not explicitly select a particular chirality, such as those mediated by RPA-screened Coulomb interactions [43, 48, 51]. In the absence of the sublattice form factors, the two chiral solutions become degenerate and the generalized clapping mode correspondingly becomes gapless.

The twofold degeneracy of the generalized clapping mode arises because coherent superpositions of the two opposite-chirality solutions may be formed and globally rotated. Importantly, these modes are charge neutral, $\sum_{\mathbf{k}} \delta \mathbf{d}_{\mathbf{k}}^{\text{GCM}} \cdot \hat{z} = 0$, and therefore do not hybridize with plasmons via the Ander-

son–Higgs mechanism. This separation allows the generalized clapping modes to be probed independently of plasma excitations. By contrast, the next set of collective modes at $\lambda \approx 0.3$ meV carries a net charge fluctuation (see Appendix) and is therefore expected to hybridize with plasmons. Together, these results establish the generalized clapping mode as a distinct, charge-neutral collective excitation associated with fluctuations of the discrete chiral order parameter. Having determined the collective-mode spectrum, we can proceed to construct the dressed photon vertex. We substitute $X_{\mathbf{k}} = -e\gamma_{\mathbf{k}} \cdot \mathbf{A}/\Delta E_{\mathbf{k}}$, $\gamma_{\mathbf{k}} \equiv \langle U_{c,+,\mathbf{k}} | \Gamma_{\mathbf{k}} | U_{c,-,\mathbf{k}} \rangle$ into Eq. (12), which yields

$$\sum_{\mathbf{k}'} \left[\delta_{\mathbf{k}\mathbf{k}'} \mathcal{I}_2 + \frac{C_{\mathbf{k},\mathbf{k}'}}{\Delta E_{\mathbf{k}'}} \right] \begin{pmatrix} \gamma_{\mathbf{k}'}^R \\ \gamma_{\mathbf{k}'}^0 \end{pmatrix} = \begin{pmatrix} \gamma_{\mathbf{k}}^0 \\ 0 \end{pmatrix}. \quad (32)$$

The dressed photon vertex $\gamma_{\mathbf{k}}$ is obtained by inverting this matrix equation. In performing this inversion, the ABG mode must be removed. In the Appendix, we provide more data to compare the resulting dressed vertex fields with the bare quasiparticle velocity field.

SUMMARY AND OUTLOOK

In this work, we have developed a microscopic framework for computing orbital magnetization in chiral superconductors that explicitly preserves gauge invariance and the associated conservation laws. While previous approaches [11, 54, 55] have provided important insights into orbital magnetization in superconducting systems, they are formulated in frameworks that do not explicitly capture the vertex-corrections of the photon vertex. These works analyze orbital magnetization either through semiclassical equations of motion for quasiparticles or through expectation values of angular-momentum operators $\mathbf{r} \times \mathbf{p}$. Although such approaches are physically transparent and well controlled in the normal state, their extension to superconductors is subtle: the relation between angular momentum and orbital magnetization is no longer straightforwardly related by a gyromagnetic factor in the superconducting state [54, 55], and it is unclear whether condensate backflow fully captures the vertex corrections [11]. Here we show that a microscopic description of orbital magnetization in a superconducting state naturally emerges from a formulation in terms of the dressed photon vertex, which guarantees charge conservation and gauge invariance. Our approach clarify the appropriate photon vertex operators for different classes of transitions, normal–normal, normal–Bogoliubov, and Bogoliubov–Bogoliubov, thereby resolving a long-standing conceptual difficulty in defining orbital magnetization in superconducting systems. The mixed normal–Bogoliubov processes changes the normal-state orbital magnetization through contributions from the entire Fermi sea, whereas the Bogoliubov–Bogoliubov processes are dominated by states near the Fermi surface. Our formalism is general and can be readily extended to other materials including three-dimensional systems and superconductivity in moiré minibands of twisted

transition-metal dichalcogenides, which are believed to be time-reversal-symmetry-breaking [56–59].

Applying our theory to rhombohedral tetralayer graphene, we find that superconductivity can either enhance or suppress the normal-state orbital magnetization, depending on the underlying band structure. This behavior is qualitatively consistent with Fig. 2b of Ref. [36], which shows that the chiral superconducting phase expands at low carrier density while remaining largely unchanged at higher density. Beyond this phenomenological agreement, we identify a doubly-degenerate generalized clapping mode, unique to chiral superconductors, and demonstrate at a microscopic level how this collective mode contributes to orbital magnetization through electromagnetic vertex dressing.

Looking forward, our analysis has assumed a superconducting ground state composed of Cooper pairs with zero center-of-mass momentum. Extending the present framework to finite-momentum pairing states or spatially inhomogeneous superconducting phases, such as vortex lattices, is conceptually straightforward and can be achieved by applying perturbation theory to quasiparticle density matrices that break translational symmetry. An equally promising direction is to solve the Bogoliubov–de Gennes Hamiltonian in the presence of a uniform external magnetic field [60–64], and to simultaneously investigate the field dependence of the orbital magnetization and the screening current. We anticipate that these extensions will further broaden the scope and applicability of our formulation.

Acknowledgment We acknowledge helpful discussions with Manfred Sigrist, Nemin Wei, Cong Xiao and Di Xiao. Material from the University of Kentucky is based upon work supported by the U.S. Department of Energy, Office of Science, Office of Basic Energy Sciences, under Award Number DE-SC-0024346

- [1] J. Bardeen, L. N. Cooper, and J. R. Schrieffer, *Theory of superconductivity*, Physical review **108**, 1175 (1957).
- [2] P. W. Anderson and P. Morel, *Generalized Bardeen-Cooper-Schrieffer states and the proposed low-temperature phase of liquid He³*, Phys. Rev. **123**, 1911 (1961).
- [3] M. McClure and S. Takagi, *Angular momentum of anisotropic superfluids*, Physical Review Letters **43**, 596 (1979).
- [4] M. Stone and R. Roy, *Edge modes, edge currents, and gauge invariance in p x+ i p y superfluids and superconductors*, Physical Review B **69**, 184511 (2004).
- [5] V. Braude and E. Sonin, *Orbital magnetic dynamics in chiral p-wave superconductors*, Physical Review B—Condensed Matter and Materials Physics **74**, 064501 (2006).
- [6] J. A. Sauls, *Surface states, edge currents, and the angular momentum of chiral p-wave superfluids*, Physical Review B—Condensed Matter and Materials Physics **84**, 214509 (2011).
- [7] Y. Tada, W. Nie, and M. Oshikawa, *Orbital angular momentum and spectral flow in two-dimensional chiral superfluids*, Physical review letters **114**, 195301 (2015).
- [8] W. Huang, E. Taylor, and C. Kallin, *Vanishing edge currents in non-p-wave topological chiral superconductors*, Physical Re-

view B **90**, 224519 (2014).

[9] S. B. Etter, A. Bouhon, and M. Sigrist, *Spontaneous surface flux pattern in chiral p -wave superconductors*, Physical Review B **97**, 064510 (2018).

[10] J. Robbins, J. F. Annett, and M. Gradhand, *Theory of the orbital moment in a superconductor*, Physical Review B **101**, 134505 (2020).

[11] C. Xiao and Q. Niu, *Conserved current of nonconserved quantities*, Physical Review B **104**, L241411 (2021).

[12] D. Ceresoli, T. Thonhauser, D. Vanderbilt, and R. Resta, *Orbital magnetization in crystalline solids: Multi-band insulators, Chern insulators, and metals*, Phys. Rev. B **74**, 024408 (2006).

[13] I. Souza and D. Vanderbilt, *Dichroic f -sum rule and the orbital magnetization of crystals*, Physical Review B—Condensed Matter and Materials Physics **77**, 054438 (2008).

[14] D. Xiao, W. Yao, and Q. Niu, *Valley contrasting physics in graphene: magnetic moment and topological transport*, arXiv preprint arXiv:0709.1274 (2007).

[15] J. Shi, G. Vignale, D. Xiao, and Q. Niu, *Quantum theory of orbital magnetization and its generalization to interacting systems*, Physical review letters **99**, 197202 (2007).

[16] D. Xiao, M.-C. Chang, and Q. Niu, *Berry phase effects on electronic properties*, Reviews of modern physics **82**, 1959 (2010).

[17] J. Zhu and C. Huang, *Magnetic-field-induced geometric response of mean-field projectors: Streda formula and orbital magnetization*, arXiv preprint arXiv:2510.07001 (2025).

[18] T. Han, Z. Lu, Y. Yao, L. Shi, J. Yang, J. Seo, S. Ye, Z. Wu, M. Zhou, H. Liu, et al., *Signatures of chiral superconductivity in rhombohedral graphene* (2024), arXiv preprint arXiv:2408.15233.

[19] H. Zhou, T. Xie, A. Ghazaryan, T. Holder, J. R. Ehrets, E. M. Spanton, T. Taniguchi, K. Watanabe, E. Berg, M. Serbyn, et al., *Half-and quarter-metals in rhombohedral trilayer graphene*, Nature **598**, 429 (2021).

[20] T. Arp, O. Sheekey, H. Zhou, C. Tschirhart, C. L. Patterson, H. Yoo, L. Holleis, E. Redekop, G. Babikyan, T. Xie, et al., *Intervalley coherence and intrinsic spin-orbit coupling in rhombohedral trilayer graphene*, Nature Physics **20**, 1413 (2024).

[21] B. A. Levitan and E. Lantagne-Hurtubise, *Trigonal warping enables linear optical spectroscopy in single-valley superconductors*, arXiv:2508.09387.

[22] P. Wölfle, *Order-parameter collective modes in $^3\text{He} - a$* , Phys. Rev. Lett. **37**, 1279 (1976).

[23] D. S. Hirashima and H. Namaizawa, *Collective modes and a theory of response of d -wave superconductors*, Journal of Low Temperature Physics **73**, 137 (1988).

[24] P. J. Hirschfeld, P. Wölfle, J. A. Sauls, D. Einzel, and W. O. Putikka, *Electromagnetic absorption in anisotropic superconductors*, Phys. Rev. B **40**, 6695 (1989).

[25] P. J. Hirschfeld, W. O. Putikka, and P. Wölfle, *Electromagnetic power absorption by collective modes in unconventional superconductors*, Phys. Rev. Lett. **69**, 1447 (1992).

[26] S. K. Yip and J. A. Sauls, *Circular dichroism and birefringence in unconventional superconductors*, Journal of Low Temperature Physics **86**, 257 (1992).

[27] H.-Y. Kee, Y. B. Kim, and K. Maki, *Collective modes and sound propagation in a p -wave superconductor: sr_2ruo_4* , Phys. Rev. B **62**, 5877 (2000).

[28] S. Higashitani and K. Nagai, *Order parameter collective modes in sr_2ruo_4* , Physica B: Condensed Matter **284-288**, 539 (2000).

[29] S. Higashitani and K. Nagai, *Electromagnetic response of a $k_x \pm ik_y$ superconductor: Effect of order-parameter collective modes*, Phys. Rev. B **62**, 3042 (2000).

[30] A. V. Balatsky, P. Kumar, and J. R. Schrieffer, *Collective mode in a superconductor with mixed-symmetry order parameter components*, Phys. Rev. Lett. **84**, 4445 (2000).

[31] D. J. Thouless, *The quantum mechanics of many-body systems* (Courier Corporation, 2013).

[32] H. Zhou, T. Xie, T. Taniguchi, K. Watanabe, and A. F. Young, *Superconductivity in rhombohedral trilayer graphene*, Nature **598**, 434 (2021).

[33] H. Zhou, L. Holleis, Y. Saito, L. Cohen, W. Huynh, C. L. Patterson, F. Yang, T. Taniguchi, K. Watanabe, and A. F. Young, *Isospin magnetism and spin-polarized superconductivity in bernal bilayer graphene*, Science **375**, 774 (2022).

[34] Y. Zhang, R. Polski, A. Thomson, É. Lantagne-Hurtubise, C. Lewandowski, H. Zhou, K. Watanabe, T. Taniguchi, J. Alicea, and S. Nadj-Perge, *Enhanced superconductivity in spin-orbit proximitized bilayer graphene*, Nature **613**, 268 (2023).

[35] C. L. Patterson, O. I. Sheekey, T. B. Arp, L. F. Holleis, J. M. Koh, Y. Choi, T. Xie, S. Xu, Y. Guo, H. Stoyanov, et al., *Superconductivity and spin canting in spin-orbit-coupled trilayer graphene*, Nature, 1 (2025).

[36] T. Han, Z. Lu, Z. Hadjri, L. Shi, Z. Wu, W. Xu, Y. Yao, A. A. Cotten, O. Sharifi Sedeh, H. Weldeyesus, et al., *Signatures of chiral superconductivity in rhombohedral graphene*, Nature **643**, 654 (2025).

[37] J. Seo, A. A. Cotten, M. Xu, O. S. Sedeh, H. Weldeyesus, T. Han, Z. Lu, Z. Wu, S. Ye, W. Xu, et al., *Family of unconventional superconductivities in crystalline graphene*, arXiv preprint arXiv:2509.03295 (2025).

[38] E. Morissette, P. Qin, H.-T. Wu, N. J. Zhang, K. Watanabe, T. Taniguchi, and J. Li, *Superconductivity, anomalous hall effect, and stripe order in rhombohedral hexalayer graphene*, arXiv preprint arXiv:2504.05129 (2025).

[39] M. Kumar, D. Waleffe, A. Okounkova, R. Tejani, K. Watanabe, T. Taniguchi, É. Lantagne-Hurtubise, J. Folk, and M. Yankowitz, *Pervasive spin-triplet superconductivity in rhombohedral graphene*, arXiv preprint arXiv:2511.16578 (2025).

[40] Y. Guo, O. I. Sheekey, T. Arp, K. Kolář, T. Charpentier, L. Holleis, B. Foutty, A. Keough, M. Kang-Chou, M. E. Huber, et al., *Flat band surface state superconductivity in thick rhombohedral graphene*, arXiv preprint arXiv:2511.17423 (2025).

[41] J. Xie, Z. Huo, Z. Chen, Z. Zhang, K. Watanabe, T. Taniguchi, X. Lin, and X. Lu, *Magnetic-field-driven insulator-superconductor transition in rhombohedral graphene*, arXiv preprint arXiv:2512.24306 (2025).

[42] H. Zhou, N. Auerbach, M. Uzan, Y. Zhou, N. Banu, W. Zhi, M. E. Huber, K. Watanabe, T. Taniguchi, Y. Myasoedov, et al., *Imaging quantum oscillations and millitesla pseudomagnetic fields in graphene*, Nature **624**, 275 (2023).

[43] H. Yang and Y.-H. Zhang, *Topological incommensurate fulde-ferrell-larkin-ovchinnikov superconductor and bogoliubov fermi surface in rhombohedral tetralayer graphene*, Physical Review B **112**, L020506 (2025).

[44] B. A. Bernevig and Y. H. Kwan, "berry trashcan" model of interacting electrons in rhombohedral graphene, arXiv preprint arXiv:2503.09692 (2025).

[45] C. Yoon, T. Xu, Y. Barlas, and F. Zhang, *Quarter metal superconductivity*, arXiv preprint arXiv:2502.17555 (2025).

[46] A. Gil and E. Berg, *Charge and pair density waves in a spin and valley-polarized system at a van-hove singularity*, arXiv preprint arXiv:2504.19321 (2025).

[47] Y.-Z. Chou, J. Zhu, and S. Das Sarma, *Intravalley spin-polarized superconductivity in rhombohedral tetralayer graphene*, Physical Review B **111**, 174523 (2025).

[48] F. Gaggioli, D. Guerci, and L. Fu, *Spontaneous vortex-antivortex lattice and majorana fermions in rhombohedral*

graphene, Physical Review Letters **135**, 116001 (2025).

[49] Y. Zhang, L. Shackleton, and T. Senthil, *Pathways from a chiral superconductor to a composite fermi liquid*, arXiv preprint arXiv:2509.21591 (2025).

[50] Z. Han, J. Herzog-Arbeitman, Q. Gao, and E. Khalaf, *Exact models of chiral flat-band superconductors*, arXiv preprint arXiv:2508.21127 (2025).

[51] M. Geier, M. Davydova, and L. Fu, *Chiral and topological superconductivity in isospin polarized multilayer graphene*, Nature Communications (2025).

[52] M. Geier, M. Davydova, and L. Fu, *Chiral and topological superconductivity in isospin polarized multilayer graphene*, arXiv preprint arXiv:2409.13829 (2024).

[53] P. W. Anderson, *Random-phase approximation in the theory of superconductivity*, Physical Review **112**, 1900 (1958).

[54] J. F. Annett, B. Györffy, and K. Wysokiński, *Orbital magnetic moment of a chiral p-wave superconductor*, New Journal of Physics **11**, 055063 (2009).

[55] J. A. D. Robbins, *Anomalous Phenomena in Chiral Superconductors*, Ph.d. thesis, University of Bristol (2019).

[56] F. Xu, Z. Sun, J. Li, C. Zheng, C. Xu, J. Gao, T. Jia, K. Watanabe, T. Taniguchi, B. Tong, *et al.*, *Signatures of unconventional superconductivity near reentrant and fractional quantum anomalous hall insulators*, arXiv preprint arXiv:2504.06972 (2025).

[57] D. Guerci, A. Abouelkomsan, and L. Fu, *From fractionalization to chiral topological superconductivity in a flat chern band*, Physical Review Letters **135**, 186601 (2025).

[58] T. Wang and M. P. Zaletel, *Chiral superconductivity near a fractional chern insulator*, arXiv preprint arXiv:2507.07921 (2025).

[59] A. Jahin and S.-Z. Lin, *Enhanced kohn-luttinger superconductivity in geometric bands*, Physical Review B **113**, 014504 (2026).

[60] M. Norman, A. MacDonald, and H. Akera, *Magnetic oscillations and quasiparticle band structure in the mixed state of type-ii superconductors*, arXiv preprint cond-mat/9410048 (1994).

[61] A. MacDonald, H. Akera, and M. Norman, *Quantum mechanics and superconductivity in a magnetic field*, Australian journal of physics **46**, 333 (1993).

[62] M. Franz and Z. Tešanović, *Quasiparticles in the vortex lattice of unconventional superconductors: Bloch waves or landau levels?* Physical Review Letters **84**, 554 (2000).

[63] K. Yasui and T. Kita, *Theory of the de haas–van alphen effect in type-ii superconductors*, Physical Review B **66**, 184516 (2002).

[64] J. M. Murray and O. Vafek, *Majorana bands, berry curvature, and thermal hall conductivity in the vortex state of a chiral p-wave superconductor*, Physical Review B **92**, 134520 (2015).